An Experimental and Numerical Study of the Tensile Behavior of PA6-GF30 under Various Environmental Conditions

Nicolae Stefanoaea
Department of Industrial Machinery and Equipment, Faculty of Engineering, "Lucian Blaga" University of Sibiu, 4 Emil Cioran Street, Sibiu, Romania
nicolae.stefanoaea@ulbsibiu.ro

Olivia-Laura Petrascu
Department of Industrial Machinery and Equipment, Faculty of Engineering, "Lucian Blaga" University of Sibiu, 4 Emil Cioran Street, Sibiu, Romania
olivia.petrascu@ulbsibiu.ro

Adrian Marius Pascu
Department of Industrial Machinery and Equipment, Faculty of Engineering, "Lucian Blaga" University of Sibiu, 4 Emil Cioran Street, Sibiu, Romania
adrian.pascu@ulbsibiu.ro (corresponding author)

Received: 7 November 2025 | Revised: 16 February 2026 | Accepted: 27 February 2026

 DOI: https://doi.org/10.48084/etasr.16096

ABSTRACT

This study analyzed the tensile behavior of PA6-GF30 composite material exposed to different environments (ambient, distilled water, cooling oil, saline solution, and UV-C radiation). Experimental tests and numerical simulations were conducted using the Finite Element Method (FEM), yielding very good correlations between the experimental and simulated results. Experimentally, the PA6-GF30 specimens showed an increase in tensile strength after immersion in distilled water (+34.00%) and saline solution (+0.28%), whereas specimens exposed to cooling oil (-6.52%) and UV-C radiation (-24.89%) exhibited reduced tensile performance. Significant differences were also observed in strain and elastic modulus across the different environments.

Keywords-polyamide composites; glass fiber reinforcement; environmental degradation; mechanical properties; finite element analysis; aging effects

I. INTRODUCTION

Polymer matrix composites reinforced with short or long glass fibers are widely used in automotive, aerospace, and industrial applications due to their high specific strength, dimensional stability, and good manufacturability. Among them, polyamide 6 (PA6) reinforced with 30% glass fibers (PA6-GF30) is one of the most commonly employed engineering materials for structural components exposed to variable environmental conditions. Despite its mechanical advantages, PA6 is a hygroscopic polymer with a strong affinity for moisture, and its properties are significantly influenced by temperature, humidity, UV radiation, and contact with various chemicals [1].

Environmental exposure can induce a series of physical and chemical degradation mechanisms, including plasticization, hydrolysis, chain scission, fiber-matrix debonding, swelling, and microcracking. Previous studies have examined individual effects, such as moisture absorption, salt exposure, or UV aging, on polyamide-based composites; however, they are often limited to one environmental factor at a time. Moreover, mechanical responses are highly dependent on the fiber orientation and specimen manufacturing method, adding further complexity to the characterization of PA6-GF30 [2].

Although the behavior of polyamides in humid or UV environments has been reported, there is a lack of integrated research evaluating PA6-GF30 in multiple adverse environments analyzed under identical conditions. Furthermore, few publications combine experimental tensile characterization with finite element modeling to validate the mechanical response of this composite material under environmental degradation [3-5]. Understanding these combined effects is essential for predicting durability and

designing reliable polymer composite components operating under fluctuating service conditions [6].

Therefore, the present study addresses these gaps by investigating the influence of distilled water, cooling oil, saline solution, and UV-C radiation on the tensile behavior of PA6-GF30. Experimental tensile tests were performed according to ISO 527-2, and the environmental effects were quantified in terms of tensile strength, strain, and elastic modulus. Additionally, a finite element model based on a multilinear isotropic hardening law was developed to correlate numerical predictions with experimental results. The results provide an integrated understanding of how different environmental conditions affect the mechanical performance of PA6-GF30, supporting improved material selection and component design in engineering applications [5, 7, 8].

II. MATERIALS AND METHODS

PA6-GF30 specimens were obtained from extruded plates supplied as semi-finished products. Water-jet cutting was selected for specimen preparation because it avoids thermal degradation, fiber-matrix alteration, and heat-affected zones, typically associated with laser cutting or mechanical milling. Punch-cutting was not suitable due to the high stiffness of the composite and the associated risk of edge cracking. All specimens (Figure 1) were manufactured according to the geometry and tolerances specified in ISO 527-2:2012 [9], which defines the requirements for uniaxial tensile testing of plastics to ensure reproducible and comparable mechanical results [10]. Tensile tests were conducted at a controlled laboratory temperature of 23 ± 2 °C and relative humidity of 50 ± 10 %, in accordance with ISO 291:2008 [11]. These conditions were maintained consistently during both specimen conditioning and mechanical testing to minimize moisture-induced variability and ensure comparability of all experimental groups.

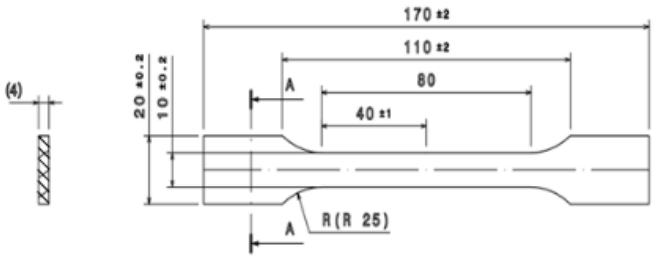

Fig. 1. PA6-GF30 specimen (dimensions in mm).

After waterjet cutting, all specimens were dimensionally inspected using a digital caliper with an accuracy of 0.01 mm to ensure compliance with ISO 527-2 tolerances. For the specimens intended for immersion in liquid environments, the initial mass was recorded using a high-precision analytical balance, enabling the subsequent evaluation of liquid absorption.

PA6-GF30 exhibits anisotropic mechanical behavior due to fiber orientation within the matrix. In this study, all specimens were cut along the extrusion direction of the semi-finished plates, ensuring consistent fiber alignment. Therefore, the reported tensile properties correspond to this principal orientation. Components with heterogeneous fiber distributions may exhibit different mechanical responses.

Tensile tests were performed using a Galdabini Quasar 25 universal testing machine. The testing method was configured in the machine's control software by defining specimen geometry, a test speed of 5 mm/min, and the acquisition parameters, including applied force (N), elongation (mm), engineering stress (MPa), and engineering strain (%), following ISO 527-2 recommendations [10, 12]. To ensure accurate axial alignment of the specimens and prevent bending-induced stress artifacts, a custom alignment fixture (Figure 2) was designed and manufactured using 3D printing. The device was employed only during positioning and removed prior to testing to prevent it from influencing the mechanical response.

Fig. 2. Test specimen attached to the test machine using the device for positioning and orientation.

Specimens for immersion in distilled water, cooling oil, or saline solution were first dried in an oven at 50 °C for 24 h, following ISO 62:2008 [13]. After complete drying, the samples were accurately weighed and then placed in the mentioned liquid media for 24 h. Uniaxial tensile mechanical testing, performed under controlled laboratory conditions, represents the primary testing medium and plays an essential role in the analysis and characterization of polymeric materials, allowing the evaluation of fundamental mechanical properties and relevant comparisons between the behaviors manifested in different environments. The second exposure medium analyzed was distilled water, supplied by Simple Quality Products, specifically used for the immersion of the test specimens. This type of distilled water is commonly encountered in various industrial applications, including dilution of windshield washer fluids and antifreeze, electrolyte battery refilling, steam generation for steam irons, or use in cooling systems of internal combustion engines. The water used in this study had a pH between 6 and 7.5 and a density of 1 g/cm^2 at 20 °C. The third test medium was cooling oil, specifically Azur-Cut brand 602.01 M-15. This oil is a mixture of mineral oil and special additives designed to withstand the high-pressure conditions characteristic of high-intensity machining operations. With a viscosity of 15 mm^2/s at 40 °C, this synthetic oil is used in industrial mechanical machining processes where efficient

cooling and lubrication are essential. The fourth test environment involved exposure to Ultra-Violet C (UV-C) radiation using a commercial germicidal lamp (UV-C + ozone, quartz tube, emission at 280 nm). The exposure was carried out for 24 h, in accordance with the conditioning duration used in ISO 62:2008 for water absorption studies, to ensure consistent comparison with the moisture-influenced reference samples. Specimens were kept at ambient laboratory conditions (23 ± 1 °C) during exposure. Immediately after the 24 h UV-C treatment, the samples were tested mechanically without an additional stabilization period. Thus, determining the behavior of polymers under UV-C radiation exposure guarantees the reliability and safety of products, especially in applications exposed to intense UV radiation. Finally, the fifth test medium used was saline solution, prepared according to ISO 16750-4:2023 [14]. This solution had a salinity concentration of 25% and a pH of 2.162, and was maintained at an immersion temperature of 0.5 °C. The preparation of the solution involved mixing 25 L of demineralized water, 8.34 kg of salt, and 30 ml of hydrochloric acid, thus creating a controlled test environment that simulates severe exposure to saline solutions. After the specimens were removed from these three liquids, they were wiped with a swab to remove excess liquid from the surface and then weighed again to determine the degree of liquid absorption in each material studied.

After completion of the drying process, each sample was weighed and then immersed in the selected test medium (distilled water, cooling oil, saline solution) or exposed to UV-C radiation for 24 h. After exposure, the specimens were weighed again to assess the liquid uptake for distilled water, cooling oil, and saline solution, according to the procedure described in ISO 62:2008. In the last step, after the drying process, the specimens were weighed once more to quantify the amount of liquid absorbed. Formula/Equation (1) was used to calculate the liquid uptake. The steps involved in preparing the specimens for testing are shown in Figure 3.

$$c = \frac{m_2 - m_1}{m_1} \times 100\% \quad (1)$$

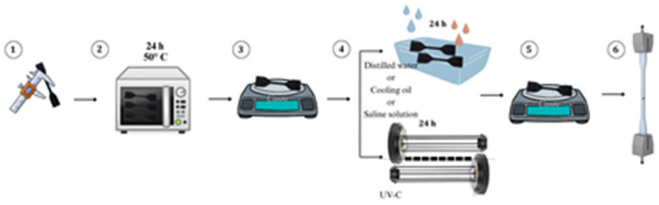

Fig. 3. Steps to perform the tensile test: 1. measuring the specimens, 2. oven drying, 3. weighing after drying, 4. immersion / exposure to the medium of interest, 5. absorption weighing, and 6. uniaxial tensile test.

III. RESULTS AND DISCUSSION

A. Experimental Results

The results obtained from the uniaxial tensile tests performed on the specimens maintained in the five environments are presented in the following section. To ensure the accuracy and relevance of the data, ten specimens were used for each medium tested (Figure 4).

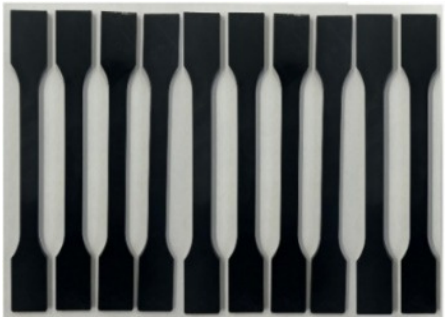

Fig. 4. Ten PA6-GF30 specimens before tensile tests.

The data collected from the five distinct groups, each composed of ten specimens, were further analyzed and interpreted. Upon completion of the tensile tests, the experimental results were subjected to statistical analysis using Minitab 18 software. This analysis focused on two key aspects: the identification of possible outliers by applying the Grubbs (G) test and the verification of the normality of the data distribution by using the Anderson-Darling (AD) test. For all sets of data, the AD and p-values for σ_{max} (maximum tensile stress), ε_{max} (maximum tensile strain), and E (elastic modulus) fall in ranges greater than 0.05, and the same is true for the Grubbs test, where the G and p-values for σ_{max}, ε_{max}, and E are greater than 0.05. This confirms that the obtained results indicate a normal distribution of the data. The results obtained from the testing in the five environments are presented in Table I, which includes the statistical indicators AD and G, as well as the p-values for these tests. The latter were selected to ensure data normality and identify potential outliers before averaging.

TABLE I. EXPERIMENTAL RESULTS (MEAN VALUES) OF THE PA6-GF30 SPECIMENS SUBJECTED TO UNIAXIAL TENSILE TESTS UNDER DIFFERENT ENVIRONMENTS

	Ambient environment	**Distilled water**	**Cooling oil**	**UV-C**	**Saline solution**
σ_{max} (MPa)	106.72	143.00	99.76	80.15	107.01
AD	0.18	0.18	0.11	0.55	0.61
Grubbs	0.23	0.28	0.55	1.00	0.97
SD	4.04	2.35	3.79	14.39	4.29
ε_{max} (%)	10.14	5.80	10.68	8.22	9.98
AD	0.49	0.42	0.59	0.31	0.14
Grubbs	0.87	1.00	0.19	1.00	0.45
SD	0.53	0.33	0.48	0.82	0.52
E (MPa)	3543.99	3564.33	3444.60	3442.86	3586.87
AD	0.64	0.52	0.46	0.38	0.52
Grubbs	0.14	0.25	0.37	1.00	0.17
SD	117.05	329.16	120.41	304.74	188.46

Based on the experimental results, the engineering stress versus engineering strain characteristic curves were plotted for each of the ten test sets in the five analyzed environments. Figure 5 shows, for each medium, an average curve plotted from the ten curves obtained for each sample tested in each case. Distilled water immersion resulted in a stiffer initial response and a higher maximum stress, whereas UV-C-exposed samples displayed the lowest strength and a noticeably more brittle behavior. Specimens immersed in cooling oil exhibited a moderate reduction in stress capacity, whereas those exposed to saline solutions behaved similarly to the

reference ambient condition. The curves illustrate how environmental exposure alters both stiffness and ductility, confirming the sensitivity of PA6-GF30 to moisture, oil contact, and UV-induced degradation.

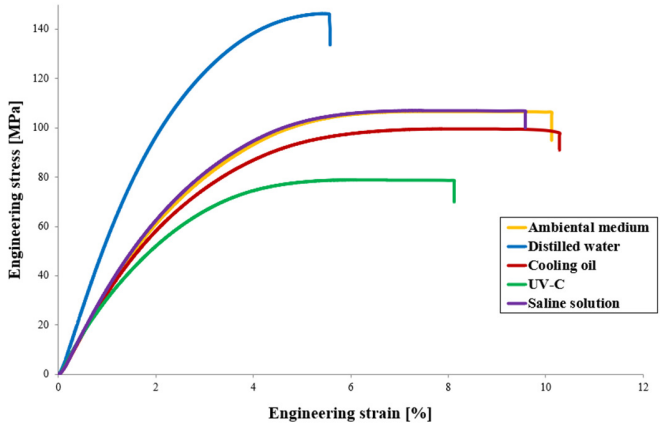

Fig. 5. Mean stress-strain derived from tensile tests of PA6-GF30 in five different environments.

Figure 6 displays a graph comparing the mean values of the maximum stress obtained for all five studied environments.

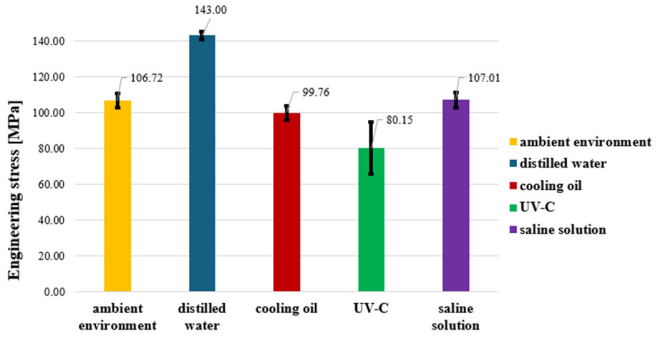

Fig. 6. Mean values of the maximum stress for PA6-GF30 specimens obtained for the five studied environments.

Figure 6 compares the mean maximum engineering stress for all environments. Distilled water produced the highest increase in tensile strength (+34.00%), primarily due to plasticization and improved fiber-matrix load transfer. This behavior is specific to short-term exposure and differs from the long-term moisture effects reported in the literature. Saline immersion caused only a slight increase (+0.28%), consistent with limited short-term hydrolysis. Cooling oil led to a modest reduction in tensile stress (-6.52%), whereas UV-C radiation resulted in the most severe decrease (-24.9%), attributable to chain scission and photo-oxidative embrittlement. This comparison highlights the contrasting mechanical responses induced by different aging mechanisms.

Therefore, the two liquid media based on water had a slight positive influence on the tensile strength of the PA6-GF30 specimens, whereas the greatest influence, this time negative, was shown by UV-C radiation, which decreased normal stress by 24.89%. The cooling oil had a slight negative influence, decreasing the maximum engineering stress by 6.52%.

From the absorption point of view, the lowest absorption percentage was observed for the cooling oil, followed by the saline solution and then the distilled water. The absorption percentages of PA6-GF30 specimens under different environmental media are presented in Table II, which includes the measured values for all 10 specimens, as well as the calculated averages. As depicted in Table II, the average absorption values were 0.36% for distilled water, 0.04% for cooling oil, and 0.26% for saline solution, indicating that distilled water leads to the highest moisture uptake while cooling oil has the least effect.

TABLE II. ABSORPTION PERCENTAGES OF PA6-GF30 SPECIMENS UNDER DIFFERENT ENVIRONMENTAL MEDIUMS

	Distilled water	**Cooling oil**	**Saline solution**
1	0.13%	0.07%	0.30%
2	0.26%	0.00%	0.00%
3	1.13%	0.00%	0.00%
4	1.05%	0.00%	0.37%
5	0.13%	0.00%	0.00%
6	0.19%	0.00%	0.07%
7	0.13%	0.00%	0.00%
8	0.26%	0.13%	0.15%
9	0.07%	0.00%	1.60%
10	0.26%	0.00%	0.07%
Average	0.36%	0.02%	0.26%

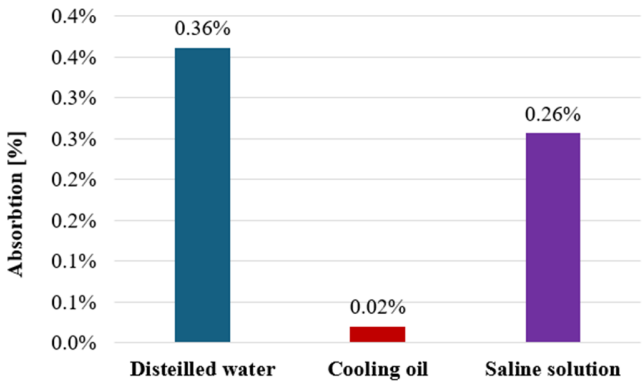

Fig. 7. Mean absorption levels in PA6-GF30 specimens for all three liquids studied.

Figure 7 presents the mean absorption levels for the three liquid environments. Distilled water showed the highest uptake (0.36%), consistent with the high hydrophilicity of PA6. Saline solution produced lower absorption due to the ionic concentration limiting further diffusion, whereas cooling oil showed minimal uptake (0.02%), indicating limited interaction between the oil and the polymer matrix. These absorption levels correlate directly with the mechanical changes observed in the tensile tests.

Figure 8 illustrates a graph comparing the mean values of the maximum engineering strain obtained for the five environments studied. In the case of specimens immersed in distilled water, a decrease (the highest) in the maximum

engineering strain of -42.80% was observed. For specimens subjected to UV-C radiation, the decrease was -18.93%. In the case of saline solution, a decrease in the maximum engineering strain of only -1.58% was noted. However, in the case of cooling oil, an increase in the maximum engineering strain of 5.28% was evidenced. It can therefore be concluded that distilled water had the most negative influence on the maximum engineering strain of the PA6-GF30 specimens, inducing a reduction in the maximum engineering strain of 42.80% compared to specimens not previously subjected to any external factor.

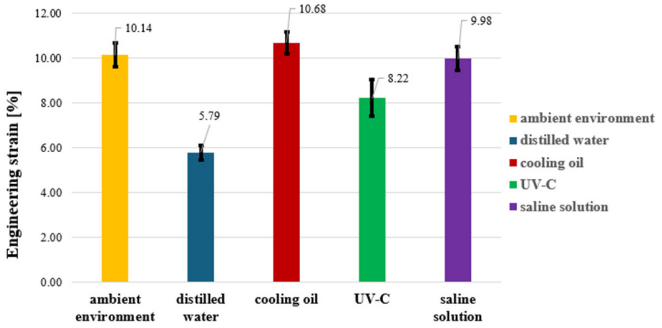

Fig. 8. Mean values of the maximum strain for PA6-GF30 specimens obtained for all five studied environments.

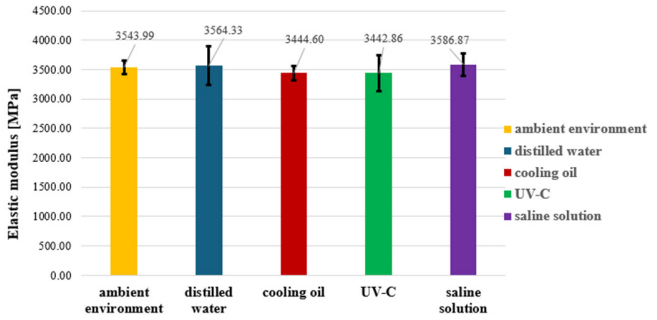

Fig. 9. Mean values of the elastic modulus for PA6-GF30 specimens obtained for all five studied environments.

Figure 9 presents a graph comparing the mean values of the maximum of the elastic modulus obtained for the five environments studied. It can be seen from this graph that, regarding the results obtained when the specimens were tested in an ambient environment without any external factor, the elastic modulus changed for the samples exposed to the test conditions. Specifically, in the case of specimens immersed in cooling oil and subjected to UV-C radiation, the elastic modulus decreased by 2.80% and 2.85%, respectively. However, the specimens immersed in distilled water showed a slight increase in the elastic modulus of 0.57%, and in the case of specimens immersed in saline solution, the increase was 1.21%. Although PA6 typically exhibits a decrease in elastic modulus upon water absorption, the observed slight increase in the elastic modulus of PA6-GF30 after short-term exposure to distilled water can be attributed to the plasticization of the PA6 matrix combined with the reinforcing effect of glass fibers. Plasticization improves the stress transfer between the matrix and fibers, temporarily enhancing stiffness [2]. This behavior is limited to short-term absorption and is followed by the expected decrease in the modulus with prolonged exposure.

B. Physical Interpretation of Tensile Behavior

The variations in the tensile strength, strain, and elastic modulus of PA6-GF30 under different environmental exposures can be explained by several microstructural mechanisms. Water absorption leads to the plasticization of the polyamide matrix, increasing ductility and facilitating stress transfer between the matrix and glass fibers, which can explain the slight increase in tensile stress observed in some cases [4, 5]. In saline solution, short-term exposure results in limited hydrolysis, causing minor reductions in tensile strength. Cooling oil interacts minimally with the polymer matrix; however, the presence of lubricating agents can reduce fiber-matrix friction, generate micro-slippage, and slightly lower tensile resistance. UV-C radiation induces chain scission and photo-oxidation, reducing the molecular weight and leading to embrittlement, which explains the significant drop in tensile stress. Microstructural analyses further suggest that exposure to these environments can cause fiber-matrix debonding, moisture-induced swelling, and microcracking, particularly in regions of stress concentration. The combination of these mechanisms underpins the observed changes in mechanical behavior, demonstrating how environmental factors affect PA6-GF30 performance [15].

The interaction between cooling oil and PA6-GF30 is primarily physical rather than chemical. Minimal absorption occurs due to the hydrophobic nature of the oil, but its presence can reduce fiber-matrix friction, leading to localized micro-slippage under tensile loading. Consequently, a slight decrease in the tensile strength and modulus may be observed, although no significant chemical degradation of the polymer matrix is expected. These findings are consistent with previous studies on polyamide composites exposed to non-polar oils, in which mechanical changes are attributed mainly to surface lubrication effects rather than polymer matrix modification.

C. Numerical Results

To simulate the uniaxial tensile behavior of specimens made of PA6-GF30 material, a 3D model of the specimen was realized using Catia V5R20 software. This model was imported into the ABAQUS software, where it was discretized into C3D8R finite elements (Figure 10), and the material data, constraints, and loads related to each test performed experimentally were applied.

Thus, the specimen was fixed (recessed) at one end, and at the opposite end, a displacement was applied in the direction of the longitudinal axis of the specimen, equal to the mean displacement recorded experimentally at the time of breakage, as portrayed in Figure 11(a).

In the numerical simulations, the maximum applied displacement corresponded to approximately 75% of the von Mises stress at failure. This level was selected because the material model did not include a fracture criterion, and applying the full experimental displacement would have

required simulating crack initiation and propagation. By limiting the stress to ~75% of the failure level, the FEM analysis remained within the calibrated plastic hardening zone, avoiding numerical divergence, and ensuring a valid comparison between experimental and simulated force-displacement curves.

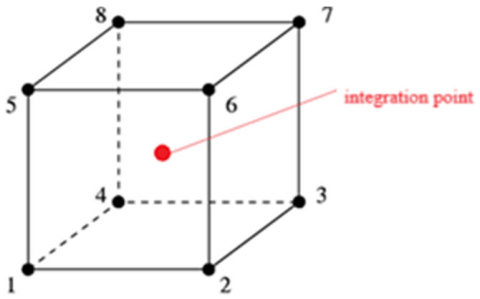

Fig. 10. C3D8R brick finite element.

Furthermore, the present numerical model does not include any damage or failure criterion. As a result, phenomena such as crack initiation, fiber-matrix debonding, or progressive material degradation cannot be reproduced in the simulation. The absence of a failure model restricts the analysis to the elastic–plastic domain. However, by limiting the applied displacement so that stresses remain within approximately 75% of the experimental failure stress, the FEM results remain stable and sufficiently accurate for comparison with the experimental force-displacement response. The discretization resulted in 16128 finite elements with approximate sizes between 0.2 and 1 mm. The distribution of the small-sized elements was concentrated in the calibrated area of the specimen, and the entire tensile specimen model had 21507 nodes. The 3D model of the tensile specimen discretized in C3D8R finite elements is presented in Figure 11(b).

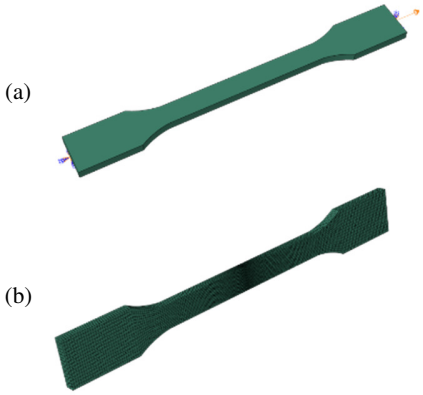

Fig. 11. 3D model of the tensile specimen.

A mesh convergence study was performed to verify the accuracy of the FEM results. Simulations with varying mesh densities, from ~8,000 to ~20,000 elements, showed convergence at ~16,128 elements, with changes in tensile stress and elastic modulus below 1%. Sensitivity checks on boundary conditions, including displacement constraints and load application points, confirmed that the numerical predictions are stable and reliable. This validated the FEM setup used in this study. Although a full mesh convergence study was not conducted, the discretization of the tensile specimen using 16,128 C3D8R elements was selected based on preliminary mesh sensitivity tests. The distribution of smaller elements in the calibrated area of the specimen ensured accurate stress and strain predictions in the region of interest. The global force-displacement response was found to be stable with minor variations (< 2%) when the mesh density was locally refined, confirming that the chosen mesh provided reliable results for comparison with the experimental data. Future work may include a more detailed mesh independence study to fully quantify numerical convergence and assess its impact on FEM predictions.

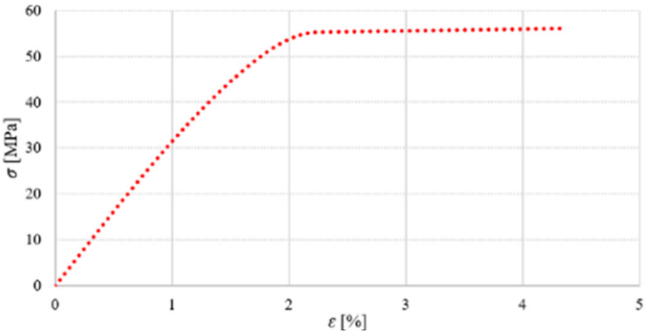

Fig. 12. Multilinear isotropic hardening model.

Based on the experimental results, mean characteristic curves (force-displacement) were plotted for the studied material. To use the multilinear isotropic hardening material model (Figure 12) in the numerical simulations, the elastic behavior of the materials was defined by the mean modulus of elasticity (E_{med} = 3970 MPa), calculated by the mean curves mentioned above, and the Poisson coefficient (ν = 0.30), which was obtained from the literature [3]. The plastic behavior of the materials was defined using stress-strain curves obtained after uniaxial tensile tests for all five studied cases.

Figures 13-17 illustrate the comparative force-displacement curves (experimental versus numerical/FEM) for specimens made of PA6-GF30 and tested under uniaxial tensile in the five studied environments, along with the distribution of the equivalent von Mises stress and the displacements in the direction of the applied load (Oz axis). From the superimposed representation of the two curves obtained experimentally and by numerical simulation for the specimens made of PA6-GF30, it can be observed that, once again, there is a very good correlation between the two curves for all five environments studied in this paper. From the representation of the equivalent stress distribution, it can be observed that in all five cases, the maximum values of this equivalent stress are recorded in the calibrated area of the specimen, marked with red color. It can also be seen that the clamping areas of the specimen are not subjected to tensile stress. The values of the maximum displacements in Figures 13-17 are related to the moment when the maximum tensile force is reached.

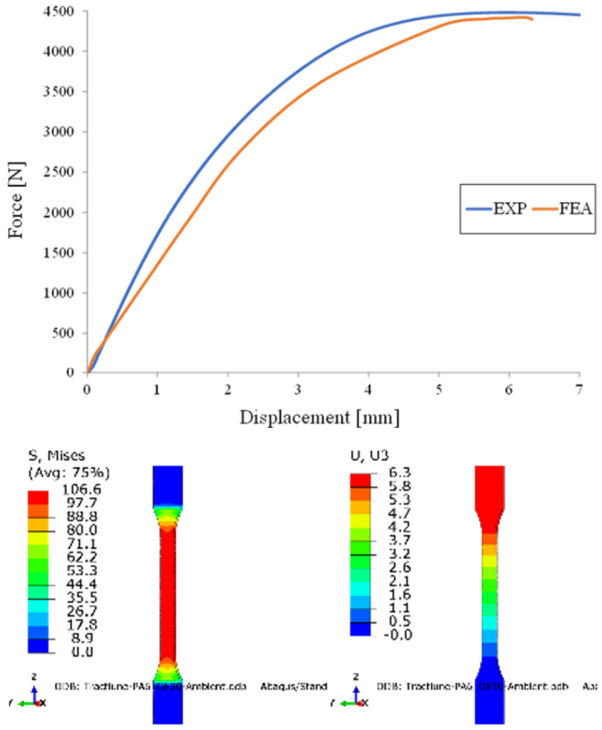

Fig. 13. Results of numerical simulation using FEM for ambient environment.

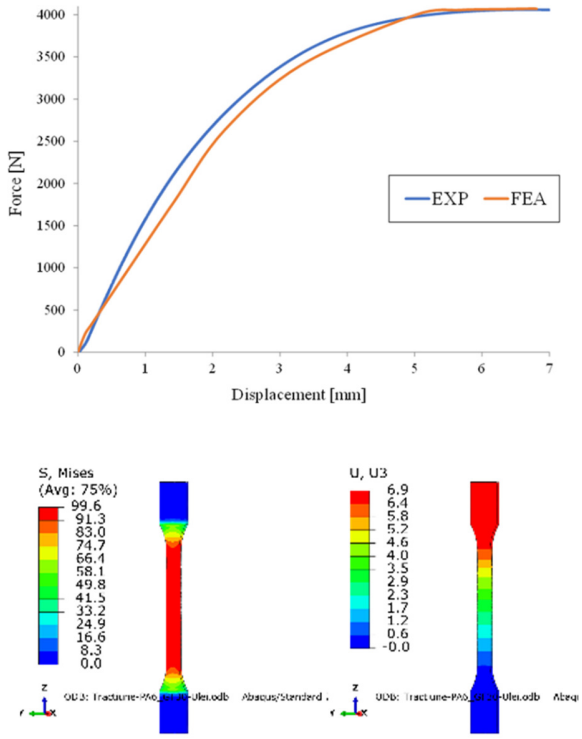

Fig. 15. Results of numerical simulation using FEM for cooling oil.

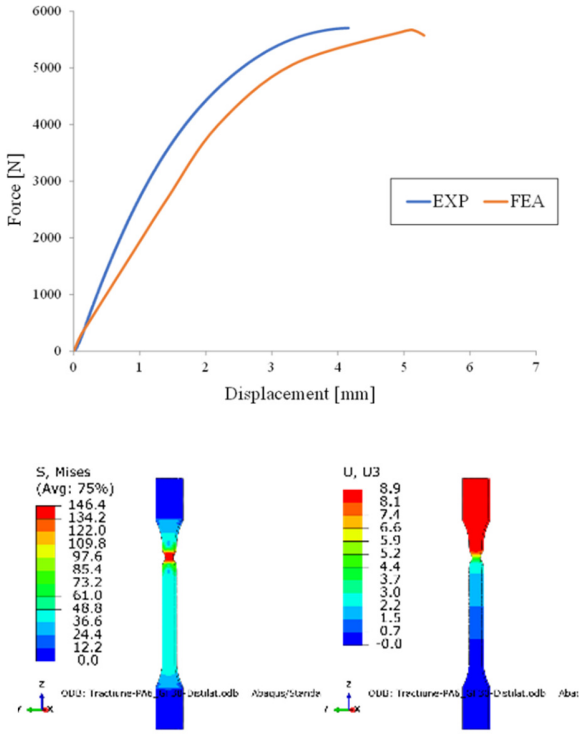

Fig. 14. Results of numerical simulation using FEM for distilled water.

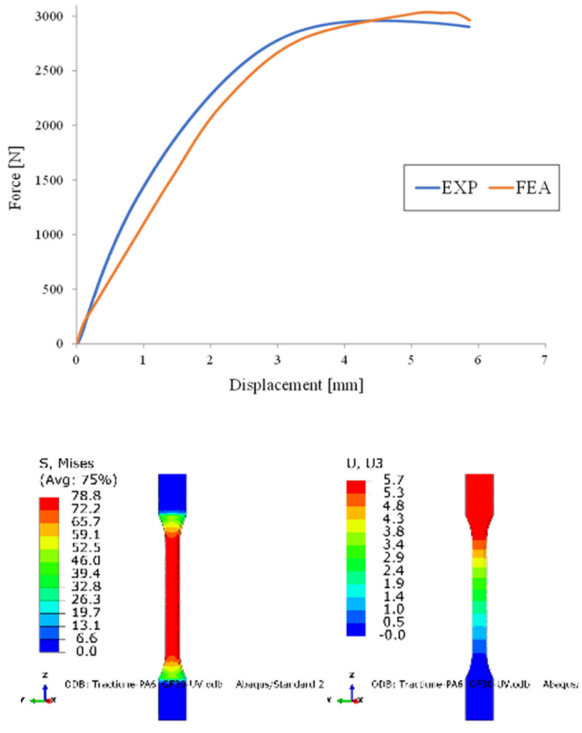

Fig. 16. Results of the numerical simulation using FEM for UV-C radiation.

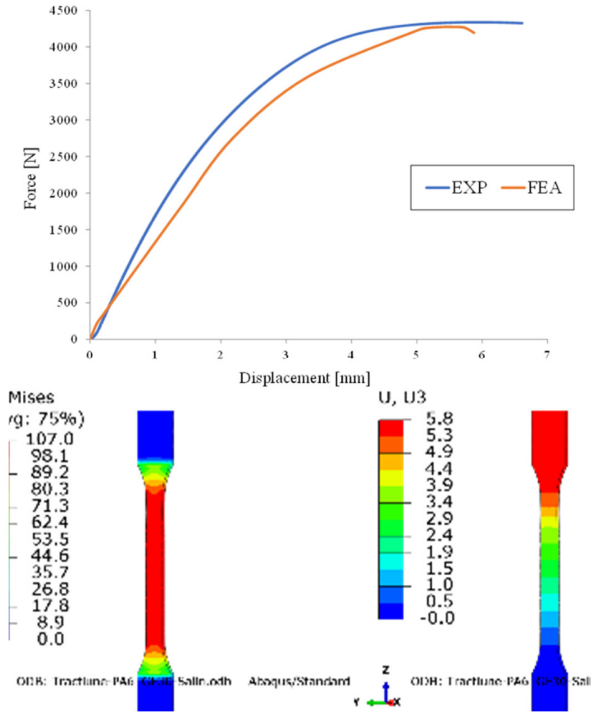

Fig. 17. Results of numerical simulation using FEM for saline solution.

IV. CONCLUSIONS

This study investigated the tensile behavior of polyamide 6 (PA6) reinforced with 30% glass fibers (PA6-GF30) exposed to different environmental conditions, and demonstrated that both the experimental results and numerical Finite Element Method (FEM) simulations are in very good agreement, with differences between 0.30% and 2.42%. Distilled water and saline solution slightly increased the tensile strength owing to plasticization and limited hydrolysis, whereas cooling oil and UV-C radiation caused notable reductions, with the latter leading to significant embrittlement through photo-oxidation. Variations in strain and elastic modulus further confirmed the sensitivity of PA6-GF30 to environmental exposure. The validated FEM model, based on a multilinear isotropic hardening law, proved capable of accurately reproducing the material response under all investigated conditions and can serve as a reliable tool for extended analyses and for predicting the mechanical performance of similar polymer composite materials.

Future studies will further investigate the long-term aging of PA6-GF30 under prolonged immersion and cyclic environmental exposure. Additionally, thermal cycling, combined chemical-mechanical degradation, and multi-axial loading conditions will be analyzed. From a numerical perspective, future FEM simulations will include progressive damage modeling and failure criteria to improve the accuracy of predicting the fracture behavior of polymeric composites.

REFERENCES

[1] J. Pospíšil, J. Pilař, N. C. Billingham, A. Marek, Z. Horák, and S. Nešpůrek, "Factors affecting accelerated testing of polymer photostability," *Polymer Degradation and Stability*, vol. 91, no. 3, pp. 417–422, Mar. 2006, https://doi.org/10.1016/j.polymdegradstab.2005.01.049.

[2] N. Stefanoaea, D. M. Rusu, and A. M. Pascu, "A Simulation Method for the One-time Snap-fit Assembly Process of PA6 GF60 - Components," *Engineering, Technology & Applied Science Research*, vol. 14, no. 1, pp. 12988–12992, Feb. 2024, https://doi.org/10.48084/etasr.6715.

[3] A. Vasile, D. M. Constantinescu, A. I. Indreș, I. C. Coropețchi, S. Sorohan, and D. A. Apostol, "Numerical Simulation of Compressive Testing of Sandwich Structures with Novel Triply Periodic Minimal Surface Cores," *Materials*, vol. 18, no. 2, Jan. 2025, Art. no. 260, https://doi.org/10.3390/ma18020260.

[4] M. Vasylius, A. Tadžijevas, D. Šapalas, V. Kartašovas, J. Janutėnienė, and P. Mažeika, "Degradation of Mechanical Properties of A-PET Films after UV Aging," *Polymers*, vol. 15, no. 20, Oct. 2023, Art. no. 4166, https://doi.org/10.3390/polym15204166.

[5] H. Webb, J. Arnott, R. Crawford, and E. Ivanova, "Plastic Degradation and Its Environmental Implications with Special Reference to Poly(ethylene terephthalate)," *Polymers*, vol. 5, no. 1, pp. 1–18, Dec. 2012, https://doi.org/10.3390/polym5010001.

[6] O. Starkova, A. I. Gagani, C. W. Karl, I. B. C. M. Rocha, J. Burlakovs, and A. E. Krauklis, "Modelling of Environmental Ageing of Polymers and Polymer Composites-Durability Prediction Methods," *Polymers*, vol. 14, no. 5, Feb. 2022, Art. no. 907, https://doi.org/10.3390/polym14050907.

[7] Mohammadi, Hamid, "Analyzing synergistic effects of combined aging environments on polymer degradation," Ph.D. dissertation, Department of Civil Engineering, Michigan State University, 2022.

[8] M. Riedl, "How Water Influences the Mechanical Properties of Polymers," *NETZSCH*, 2020. https://analyzing-testing.netzsch.com/en-US/blog/2020/how-water-influences-the-mechanical-properties-of-polymers.

[9] *ISO 527-2:2012 Plastics - Determination of tensile properties*. International Organization for Standardization, 2012.

[10] S. Shelare, K. Aglawe, S. Giri, and S. Waghmare, "Additive Manufacturing of Polymer Composites: Applications, Challenges and opportunities," *Indian Journal of Engineering and Materials Sciences*, vol. 30, no. 6, pp. 872–872, Dec. 2023, https://doi.org/10.56042/ijems.v30i6.4490.

[11] *ISO 291:2008 Plastics - Standard atmospheres for conditioning and testing*. International Organization for Standardization, 2008.

[12] B. M. Tymrak, M. Kreiger, and J. M. Pearce, "Mechanical properties of components fabricated with open-source 3-D printers under realistic environmental conditions," *Materials & Design*, vol. 58, pp. 242–246, June 2014, https://doi.org/10.1016/j.matdes.2014.02.038.

[13] *ISO 62:2008 Plastics - Determination of water absorption*. International Organization for Standardization, 2008.

[14] *ISO 16750-4:2023 Road vehicles - Environmental conditions and testing for electrical and electronic equipment*. International Organization for Standardization, 2023.

[15] M. M. Rahman *et al.*, "Polymer Composites in Additive Manufacturing: Current Technologies, Applications, and Emerging Trends," *Polymers*, vol. 18, no. 2, Jan. 2026, Art. no. 192, https://doi.org/10.3390/polym18020192.